$LaSrCr_xNi_{1-x}O_{4+\delta}$: Crystal Chemistry, Magnetism, and the Stabilization of Ni^I in an Oxide Environment

J. E. Millburn and M. J. Rosseinsky*

Inorganic Chemistry Laboratory, University of Oxford, South Parks Road, Oxford, OX1 3QR, U.K.

Received July 3, 1996. Revised Manuscript Received November 18, 1996[⊗]

Magnetic, structural and reduction data on the K_2NiF_4 structure Cr^{III}/Ni^{III} oxides, $LaSrCr_xNi_{1-x}O_{4+\delta}$ ($0.1 \le x \le 0.9$, where δ may be negative) are reported; samples with $x > 0.2$ adopt the tetragonal $I4/mmm$ space group, while for $x \le 0.2$, the samples are multiphasic due to competition between a novel vacancy-ordered $Immm$ structure and the undistorted K_2NiF_4 phase. Magnetic studies in the temperature range $5 \le T/K \le 300$ show spin glass behavior for $x < 0.9$, with freezing temperatures of between 12 and 16 K: at higher temperature the susceptibilities display Curie−Weiss behavior. The magnetism of the $x = 0.9$ sample resembles that reported for $LaSrCrO_4$, displaying an antiferromagnetic transition at 150 K and weak ferromagnetism below 130 K. Reduction of the title compounds in 1 atm of flowing H_2 at ~500 °C produces stable, oxygen-deficient compounds, notably $La_2Sr_2CrNiO_7$, which contains Ni^I with a thermal stability unprecedented in an oxide.

Introduction

In this paper, we describe the effect of Cr^{III} substitution on the crystal structure, magnetism, and chemical reactivity of $LaSrNiO_4$, an important member of the $La_{2-x}Sr_xNiO_{4\pm\delta}$ solid solution. The reduction chemistry of the new $LaSrCr_xNi_{1-x}O_{4+\delta}$ phases allows access to a novel, stable Ni^I oxide. This study of Cr^{III}/Ni^{III} oxides allows evaluation of the effect of localized competing exchange interactions on the two-dimensional square-planar lattice, providing a reference point for the pure nickelate systems in the localized electron limit.

The Ni^{II}/Ni^{III} $La_{2-x}Sr_xNiO_{4\pm\delta}$ oxides with the K_2NiF_4 structure have been the focus of much recent research.[1−10] Much higher doping levels are required to induce metal−insulator transitions in the nickel system than in the analogous cuprates, $La_{2-x}Sr_xCuO_{4\pm\delta}$, with truly metallic behavior occurring only at nickel oxidation states higher than +III. The electronic properties of the intermediate phases are intriguing—"charge ordering" transitions in which polaronic carriers are localized in superlattice arrays occur at a variety of temperatures in a narrow concentration range around $x = 0.33$,[7,8] and the low-temperature dc magnetization of the insulating phases is characteristic of spin glasses, while complex magnetic structures involving "stripe" ordering are seen by neutron diffraction and μSR reveals reduced spin freezing temperatures.[1,2,5] Introduction of Ni^{III} by oxidation is expected to produce magnetic interactions that will compete with the antiferromagnetic ground state of La_2NiO_4.

The possible correspondence in oxide chemistry between the isoelectronic Cu^{II} and Ni^I oxidation states, both of which correspond to a $3d^9$ electronic configuration, has not been widely investigated. Ni^I is rare in oxides but is found as the phosphine complex $Ni(PPh_3)_4^+$ and may be stabilized within faujasitic zeolite supercages.[11−13] The possibility of preparing Ni^I oxides with greater thermal stability than the previously reported compounds, $LaNiO_2$,[14] $YSr_5Ni_3O_8$,[15] and MNa_2NiO_2 (M = Rb, K),[16] which has linear coordination of oxygen to nickel, is both chemically interesting and potentially important in the search for new superconducting oxides. The former two examples of the Ni^I oxidation state in oxides were prepared by topotactic hydrogen reduction of ternary Ni^{III} oxides and rely upon the kinetic stabilization of the Ni^I state at low temperatures, so that the thermodynamically favored reduction to nickel metal is sufficiently slow to allow isolation of the intermediate Ni^I phase. The problem with these current approaches to Ni^I oxides is the limited thermal stability of the compounds—$LaNiO_2$ is stable only over a very narrow

[⊗] Abstract published in *Advance ACS Abstracts,* January 15, 1997.

(1) Chow, K. H.; Pattenden, P. A.; Blundell, S. J.; Hayes, W.; Pratt, F. L.; Jestadt, T.; Green, M. A.; Millburn, J. E.; Rosseinsky, M. J.; Hitti, B.; Dunsiger, S. R.; Kiefl, R. F.; Chen, C.; Chowdhury, A. J. S. *Phys. Rev. B, Rapid Commun.* **1996**, *53*, 14725−14728.

(2) Sachan, V.; Buttrey, D. J.; Tranquada, J. M.; Lorenzo, J. E.; Shirane, G. *Phys. Rev. B* **1995**, *51*, 12742−12746.

(3) Pellegrin, E.; Zaanen, J.; Lin, H. J.; Meigs, G.; Chen, C. T.; Ho, G. H.; Eisaki, H.; Uchida, S. *Phys. Rev. B* **1996**, *53*, 10667−10679.

(4) Takeda, Y.; Kanno, R.; Sakano, M.; Yamamoto, O.; Takano, M.; Bando, Y.; Akinaga, H.; Takita, K.; Goodenough, J. B. *Mater. Res. Bull.* **1990**, *25*, 293−306.

(5) Strangfeld, T.; Westerholt, K.; Bach, H. *Physica C* **1991**, *183*, 1−10.

(6) Kato, M.; Maeno, Y.; Fujita, T. *Physica C* **1991**, *176*, 533−540.

(7) Cheong, S.-W.; Hwang, H. Y.; Chen, C. H.; Batlogg, B.; Rupp, L. W.; Carter, S. A. *Phys. Rev. B, Rapid Commun.* **1994**, *49*, 7088−7091.

(8) Chen, C. H.; Cheong, S.-W.; Cooper, A. S. *Phys. Rev. Lett.* **1993**, *71*, 2461−2464.

(9) Cava, R. J.; Batlogg, B.; Palstra, T. T. M.; Krajewski, J. J.; Peck, W. F.; Ramirez, A. P.; Rupp, L. W. *Phys. Rev. B, Rapid Commun.* **1991**, *43*, 1229−1232.

(10) Granados, X.; Fontcuberta, J.; Vallet-Regi, M.; Sayagues, M. J.; Gonzalez-Calbet, J. M. *J. Solid State Chem.* **1993**, *102*, 455−464.

(11) Garbowski, E.; Vedrune, J. C. *Chem. Phys. Lett.* **1977**, *48*, 550−554.

(12) Olivier, D.; Richard, M.; Che, M. *Chem. Phys. Lett.* **1978**, *60*, 77−80.

(13) Olivier, D.; Richard, M.; Bozon-Verduraz, F.; Clarkson, R. B. *J. Chem. Phys.* **1980**, *84*, 420−422.

(14) Crespin, M.; Levitz, P.; Gatineau, L. *J. Chem. Soc., Faraday Trans.* **1983**, *79*, 1181−1203.

(15) James, M.; Attfield, J. P. *J. Chem. Soc., Chem. Commun.* **1994**, *10*, 1185−1186.

(16) Burow, W.; Birx, J.; Bernhardt, F.; Hoppe, R. *Z. Anorg. Allg. Chem.* **1993**, *619*, 923−933.

S0897-4756(96)00357-2 CCC: $14.00

temperature window during synthesis ($570 < T/K < 670$[14]). In this work we show that cosubstitution of electropositive species (the parent all-chromium oxides of the solid solution discussed here are stable with respect to reduction below the +III oxidation state under 1 atm of flowing hydrogen below 800 °C[17]) onto the octahedral site of the perovskite structure together with nickel allows the preparation of well-defined Ni^{I} oxides with unprecedented thermal stabilities. Indeed, the $x = 0.5$ material undergoes reduction to form a Ni^{I} oxide stable in reducing atmospheres up to 950 °C, showing that this cosubstitution onto the octahedral sites of the perovskite is a good strategy to enhance the kinetic stability of Ni^{I} oxides. The tolerance of the Cr/Ni substituted K_2NiF_4 structure for high concentrations of oxygen vacancies allows the observation of a vacancy-ordered *Immm* phase at $x \leq 0.2$, where the Ni^{III} oxidation state cannot be stabilized under the synthesis conditions.

Previous studies of the substitution of chromium for nickel in ternary oxide systems have concentrated on the three dimensional perovskite solid solution $LaNi_{1-x}Cr_xO_3$.[18−20] For low values of x these compounds adopt the rhombohedral structure of $LaNiO_3$ but become orthorhombic for $x > 0.35$.[19] The $x = 0$ member of the series, $LaNiO_3$, is metallic, while the $x = 1.0$ member, $LaCrO_3$, is an insulator, and the resistivity is found to increase progressively with increasing chromium content, a composition-controlled metal−insulator transition occurring in the range $0.05 < x < 0.10$. Here we demonstrate that considerable attention to the precise synthetic conditions and detailed confirmation of single phase behavior by Rietveld analysis of high-quality powder X-ray diffraction data is required for the synthesis of pure phases in the two-dimensional K_2NiF_4 structure.

Experimental Section

Stoichiometric quantities of La_2O_3 (99.999%, Aldrich, dried in air at 800 °C) $SrCO_3$ (99.994%, Alfa), Ni powder (99.999%, Aldrich), and $Cr(NO_3)_3 \cdot 9H_2O$ (99.99%, Aldrich) were dissolved in a minimum quantity (typically 150 mL) of a 1:1 solution of analar 6 M nitric acid and distilled water. Analar ethylene glycol (5 mL, 99.5%, BDH) and 1 equiv of citric acid/mol of M^{3+} cation (99.5%, BDH) were added, and the solutions heated at 150 °C on a hot plate with constant stirring for approximately 3 h. The gel formed was decomposed by further heating at 300 °C for ∼24 h. The resulting powder was ground, returned to the furnace in air at 800 °C for between 24 and 48 h, and then pressed into 13 mm diameter pellets at 10 tons. The pellets were annealed at between 1200 and 1300 °C in 1 atm of flowing argon (dried by passage over activated molecular sieves) for 6−8 days with several intermittent grindings. The black, polycrystalline solid products were allowed to cool under the argon flow at the rate of the furnace, typically 12 h, before being removed. Precise synthetic details, which are very important in the isolation of pure phases, are given in Table 1.

The Ni^{III} content of the samples thus prepared was determined by iodometric titration against a standardized potassium thiosulfate solution, the titrations being repeated several times to ensure accurate and consistent results.[21] The thiosulfate solution was standardized against the primary standard potassium iodate. [22]

Table 1. Precise Synthesis Conditions for $LaSrCr_xNi_{1-x}O_{4+\delta}$, $La_{0.9}Nd_{0.1}SrCr_{0.5}Ni_{0.5}O_4$ and $NdCaCr_{0.5}Ni_{0.5}O_4$

x	synth temp/°C (gas atmosphere, time/h)
0.1	400 (air, 24); 800 (air, 72); 1200 (Ar, 90); 1300 (90)
0.2	400 (air, 72); 800 (air, 48); 1200 (Ar, 90); 1250 (Ar, 43); 1200 (Ar, 90)
0.3	400 (air, 18); 800 (air, 48); 1200 (Ar, 90); 1250 (Ar, 42)
0.4	400 (air, 72); 800 (air, 48); 1200 (Ar, 90); 1300 (Ar, 90); 1250 (Ar, 42)
0.5	300 (air, 24); 800 (air, 72); 1200 (Ar, 20); 1200 (Ar, 40)
0.55	350 (air, 24); 800 (air, 48); 1250 (Ar, 90); 1250 (40)
0.6	350 (air, 48); 800 (air, 72); 1200 (Ar, 90); 1300 (Ar, 90)
0.7	400 (air, 24); 800 (air, 96); 1200 (Ar, 90); 1300 (Ar, 90)
0.8	400 (air, 72); 800 (air, 48); 1200 (Ar, 90)
0.9	400 (air, 72); 800 (air, 48); 1200 (Ar, 90)
$La_{0.9}Nd_{0.1}SrCr_{0.5}Ni_{0.5}O_4$	250 (air, 72); 350 (air, 24); 850 (air, 48); 1250 (Ar, 96)
$NdCaCr_{0.5}Ni_{0.5}O_4$	450 (air, 24); 950 (air, 96); 1300 (Ar, 96)

[a] The conditions for each step are given in the format: temperature in °C (gas atmosphere, time in hours).

Powder X-ray diffraction data were collected in Bragg−Brentano geometry on a Siemens D5000 diffractometer (Cu $K\alpha_1$ radiation) in 0.02° steps, the samples being mounted on a silicon wafer. Crystal structure analysis was performed with the Rietveld method using the GSAS program suite.[23,24] A cosine Fourier series background and a pseudo-Voigt peak shape function were employed. In the single-phase fits, refinement was terminated when the agreement indices for the Rietveld refinement were comparable with those for a LeBail intensity extraction "model-free" fit to the data,[25] confirming that the fit was close to the best which could be attained by profile refinement. Refinement of the data collected for the $x = 0.1$ sample was carried out using the FullProf refinement program incorporating a pseudo-Voigt peak shape[26] and a polynomial background function, as this allowed computation of an anisotropic peak shape function in which the width of a Bragg reflection depends on its Miller indices. [27]

Magnetic susceptibility measurements were performed with a Quantum Design MPMS SQUID magnetometer in the range $5 \leq T/K \leq 300$ in a 0.1 T field, for $La_{0.9}Nd_{0.1}SrCr_{0.5}Ni_{0.5}O_4$ and samples with $x = 0.3$, 0.5, 0.7, and 0.9. The data for the $x = 0.55$ and $NdCaCr_{0.5}Ni_{0.5}O_4$ samples were collected over the same temperature range in 0.01 and 0.5 T fields using a Cryogenics Consultants SCU500 SQUID magnetometer.

Thermogravimetric analysis was carried out using a Rheometric Scientific STA 1500 thermal analyzer. Samples weighing approximately 50 mg contained in platinum crucibles were

(17) Morales Sanchez, A.; Fernandez, F.; Saez Puche, R.; Fernandez-Martin, F. *J. Alloys Compounds* **1994**, *203*, 143−148.
(18) Jin, F.; Endo, T.; Takizawa, H.; Shimada, M. *J. Solid State Chem.* **1994**, *113*, 138−144.
(19) Ganguly, P.; Vasanthacharya, N. Y.; Rao, C. N. R.; Edwards, P. P. *J. Solid State Chem.* **1984**, *54*, 400−406.
(20) Hofer, H. E.; Kock, W. E. *J. Electrochem. Soc.* **1993**, *140*, 2889−2894.
(21) Karppinen, M.; Fukuoka, A.; Niinisto, L.; Yamauchi, H. *Superconduct. Sci. Technol.* **1996**, *9*, 121−135.
(22) Vogel, A. I. *A Textbook of quantitative inorganic analysis*; 3rd ed.; Longmans: London, 1961.
(23) Rietveld, H. M. *J. Appl. Crystallogr.* **1969**, *2*, 65−71.
(24) Larson, A. C.; Von Dreele, R. B. *General Structural Analysis System*; Los Alamos National Laboratory, 1990.
(25) Cox, D. E. In *Synchrotron Radiation Crystallography*; Academic Press: London, 1992.
(26) Thompson, P.; Cox, D. E.; Hastings, J. B. *J. Appl. Crystallogr.* **1987**, *20*, 79−83.
(27) Rodriguez-Carvajal, J.; Fernandez-Diaz, M. T.; Martinez, J. L. *J. Phys.−Condens. Matter* **1991**, *3*, 3215−3234.

Table 2. Structural Parameters of $LaSrCr_xNi_{1-x}O_{4+\delta}$ Obtained from Rietveld Refinement of Powder X-ray Diffraction Data[a]

	x	0.3	0.5	0.7	0.8	0.9
	δ	−0.08	−0.02	0.03	0.04	0.04
	a (Å)	3.81486(5)	3.82605(3)	3.84398(9)	3.85061(4)	3.85713(4)
	c (Å)	12.6554(1)	12.6327(1)	12.5829(3)	12.5497(1)	12.5195(1)
	V (Å^3)	184.176	184.925	185.927	186.083	186.255
La/Sr	z	0.3590(1)	0.35854(6)	0.3591(1)	0.35891(6)	0.35918(8)
	U_{iso} (Å^2)	0.0175(3)	0.02	0.02	0.0132(3)	0.0111(3)
Cr/Ni	U_{iso} (Å^2)	0.0201(8)	0.02	0.02	0.0157(7)	0.0102(8)
O(1)	z	0.1721(6)	0.1715(4)	0.1667(6)	0.1659(4)	0.1664(6)
	U_{iso} (Å^2)	0.028(2)	0.02	0.02	0.013(1)	0.018(2)
O(2)	U_{iso} (Å^2)	0.034(3)	0.02	0.02	0.015(2)	0.013(2)
	R_{wp} (%)	10.1	9.9	9.6	10.0	9.6
	R_p (%)	7.6	7.7	7.7	7.8	7.4
	R_F^2 (%)	8.3	8.3	9.4	8.4	8.6
	R_F (%)	5.0	4.6	5.4	4.3	5.0
	χ^2	1.4	1.6	1.4	1.4	1.2

[a] Thermal parameters were fixed in some cases as described in the text. The atoms were refined in the following Wyckoff positions of space group No. 139, $I4/mmm$:

4(La/Sr) and 4O(1)	in (e)	(4 mm)	(0,0,z)
2(Ni/Cr)	in (a)	(4/mmm)	(0,0,0)
4 O(2)	in (c)	(mmm)	(0,$^1/_2$,0)

placed in the apparatus which was then purged for at least 30 min with H_2, predried over activated molecular sieves. Samples were subsequently heated to 800 °C at a rate of 5 °C min^{-1} under the gas flow and held at this temperature for up to 2 h before being allowed to cool to room temperature at the cooling rate of the furnace.

Results

Synthesis Conditions. The exact temperature, gas atmosphere and length of reaction were found to be crucial in obtaining pure product phases containing no traces of the starting materials. This statement is true to a very much greater extent than is the case for the synthesis of the end-member all-chromium and all-nickel oxides. Preparation in air or pure oxygen, or for too short a period of time, resulted in the presence of La_2O_3 as an impurity, indicative of the oxidation of Cr^{III} to Cr^{IV} in the layered perovskite phase. However, reaction for too great a length of time, or at too high a temperature, in argon resulted in the presence of NiO as an impurity, indicating reduction of Ni^{III} to Ni^{II} is thermodynamically favored under these synthesis conditions. The $x = 0.5$ sample, with equal concentrations of chromium and nickel, was particularly sensitive to the exact synthesis conditions, and we therefore attempted to stabilize this composition through adjustment of the unit cell size, by carrying out substitutions at the A cation site: the compounds $La_{0.9}Nd_{0.1}SrCr_{0.5}Ni_{0.5}O_4$ and $NdCaCr_{0.5}Ni_{0.5}O_4$ were indeed easier to prepare phase pure and less sensitive to the synthesis conditions than their lanthanum/strontium analogues, the heating times and temperatures being far less critical to the production of monophasic samples. The exact synthesis conditions employed to prepare each sample are given in Table 1. Inspection of the X-ray patterns at intermediate stages of the syntheses appeared to indicate phase purity, but peculiar peak shapes were evident from Rietveld refinement of the patterns, indicating a truly single phase had not been formed. Confirmation of successful synthesis requires a satisfactory single-phase Rietveld refinement.

Iodometry. Samples with $x \geq 0.7$ and those containing neodymium dissolved in aqueous acid too slowly for reliable iodometric analysis of the oxygen content of these compounds. The results of the titrations performed upon the remaining members of the solid solution are given in Tables 2 and 3, and a plot of oxygen content and average transition-metal oxidation state against x in $LaSrCr_xNi_{1-x}O_{4+\delta}$ can be found in Figure 1.

X-ray Powder Diffraction. The crystal structures of samples with $0.3 \leq x \leq 0.9$ were refined, from powder X-ray data, in the $I4/mmm$ tetragonal space group; this is the same space group adopted by the parent compounds $LaSrCrO_4$ and $LaSrNiO_4$.[4,28] The positional and thermal parameters obtained are shown in Table 2. For the $x = 0.5$ and $x = 0.7$ samples, physically sensible isotropic temperature factors could not be refined and so the values were fixed, at 0.02 Å^2, in the final refinements. For other values of x, isotropic temperature factors were successfully refined for the oxygen sites and metal sites. It proved impossible to refine the Ni/Cr ratio, due to the similar X-ray scattering powers of these elements, while refinement of the oxygen site occupancies proved unstable and made no difference to the quality of the fits, illustrating the insensitivity of powder X-ray diffraction to the small variations in oxygen content indicated for these compounds by iodometry. The observed, calculated and difference profiles for the refinement of $LaSrCr_{0.8}Ni_{0.2}O_4$ are shown in Figure 2.

The X-ray pattern of the $x = 0.1$ sample showed splitting of some Bragg reflections which was indicative of an orthorhombic unit cell. Two distortions of the $I4/mmm$ K_2NiF_4 aristotype cell to orthorhombic symmetry are known, depending on which of the ⟨100⟩ and ⟨110⟩ sets of mirror planes and 2-fold axes are lost together with the 4-fold axis when the symmetry is lowered. The most commonly observed symmetry lowering involves a doubling of the cell size in a $(\sqrt{2}a) \times (\sqrt{2}b) \times c$ superstructure, with a 45° rotation about c in which the face diagonals of the $I4/mmm$ cell become the new cell vectors and the ⟨100⟩ mirror planes are lost. The signature of this symmetry-lowering in powder diffraction is a splitting of the tetragonal $\{hhl\}$ (into $\{2h, 0, l\}$ and $\{0, 2h, l\}$) and $\{hkl\}$ reflections (into $\{h + k, h - k, l\}$ and $\{h - k, h + k, l\}$) while the $\{h0l\}$ reflections

(28) Joubert, J. C.; Collomb, A.; Elmaleh, D.; Le Flem, G.; Daoudi, A.; Ollivier, G. *J. Solid State Chem.* **1970**, *2*, 343−346.

Table 3. Structural Parameters Obtained from Multiphase Rietveld Refinements of Powder X-ray Diffraction Data for $LaSrCr_{0.1}Ni_{0.9}O_{4+\delta}$ and $LaSrCr_{0.2}Ni_{0.8}O_{4+\delta}$[a]

		$LaSrCr_{0.1}Ni_{0.9}O_{4+\delta}$ (δ −0.25)		$LaSrCr_{0.2}Ni_{0.8}O_{4+\delta}$ (δ −0.19)	
		Immm	*I*4/*mmm*	Immm	*I*4/*mmm*
	a (Å)	3.8385(1)	3.8005(2)	3.8164(1)	3.8085(1)
	b (Å)	3.7645(1)	3.8005(2)	3.8006(1)	3.8085(1)
	c (Å)	12.6587(4)	12.6593(9)	12.6627(5)	12.6619(6)
	V (Å^3)	182.93	182.87	183.67	183.66
	fraction (%)	61.1(1)	38.8(1)	58.1(1)	41.8(1)
La/Sr	*z*	0.3597(2)	0.3586(5)	0.3580(5)	0.3605(7)
	U_{iso} (Å^2)	0.025(6)	0.081(3)	0.026(1)	0.020(2)
Cr/Ni	U_{iso} (Å^2)	0.029(2)	0.079(4)	0.051(4)	0.002(4)
O(1)	*z*	0.165(1)	0.181(4)	0.167(3)	0.176(6)
	U_{iso} (Å^2)	0.070(6)	0.076(9)	0.017(9)	0.04(1)
	occupancy	1.0	1.0	1.0	1.0
O(2)	U_{iso} (Å^2)	0.031(9)	0.096(9)	0.02	0.02
	occupancy	0.65(2)	0.875	0.78(3)	0.905
O(3)	U_{iso} (Å^2)	0.036(5)		0.02	
	occupancy	1.09(2)		1.02(3)	
	R_{wp} (%)	10.0		10.4	
	R_p (%)	7.8		8.0	
	R_F^2 (%)			8.2	
	R_F (%)	5.98	5.5	4.8	3.7
	χ^2	1.3		1.3	

[a] The atoms were refined in the following Wyckoff positions of space group No. 71, *Immm*:

4(La/Sr) and 4O(1)	in (i)	(*mm*2)	(0,0,*z*)
2(Ni/Cr)	in (a)	(*mmm*)	(0,0,0)
2O(2)	in (d)	(*mmm*)	(0,$^1/_2$,0)
2O(3)	in (b)	(*mmm*)	($^1/_2$,0,0)

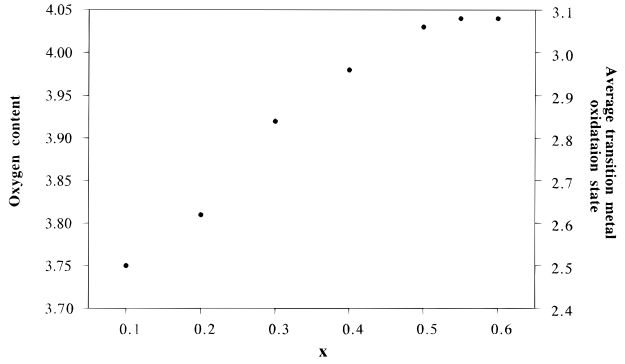

Figure 1. Oxygen content and average transition-metal oxidation state versus *x* in $LaSrCr_xNi_{1-x}O_{4+\delta}$.

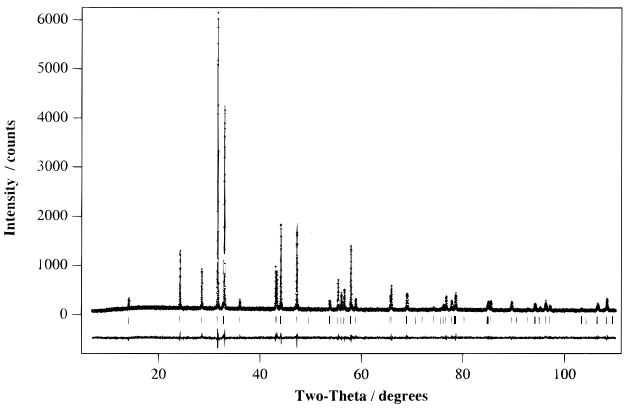

Figure 2. Observed (markers), calculated (line), and difference profiles for the X-ray Rietveld refinement of $LaSrCr_{0.8}Ni_{0.2}O_{4+\delta}$ in the *I*4/*mmm* space group.

remain unsplit (as {*h h l*} in the enlarged cell). This is found in the analogous high-temperature superconducting cuprates, in $La_2NiO_{4\pm\delta}$[27] and many other K_2NiF_4 structure oxides and results in structures with the space groups *Cmca* (tilting of MO_6 octahedra through a small angle about the *b* axis) or *Fmmm* (positive distortion of the MO_6 octahedra along the *b* direction). Inspection of the X-ray pattern of $LaSrNi_{0.9}Cr_{0.1}O_{3.75}$ indicates that this is not the case: Figure 3a shows that the *I*4/*mmm* {103} reflection splits while the {110} does not. An alternative distortion results in the loss of the ⟨110⟩ mirror planes and produces an orthorhombic cell of the same volume in which the *a* and *b* cell directions are retained but are now no longer equivalent in magnitude. Such a distortion has been reported for the mixed-valence, reduced nickelates, $La_{1.6}Sr_{0.4}(Ni^{I}, Ni^{II})O_{3.47}$[29] and $LaSr(Ni^{I}, Ni^{II})O_{3.1}$,[30] where the oxygen vacancies are found solely in the NiO_x planes, leading to a lowering of the nickel coordination number from six (octahedral) to a mixture of five (square pyramidal) and four (square planar). These compounds have orthorhombic symmetry due to the oxygen vacancies preferentially occurring along one axis within the MO_x layers. In this case the {*hhl*} reflections, corresponding to the diagonal of the unit cell, remain unsplit, whereas the {*h*0*l*} split into {0*hl*} and {*h*0*l*} The observation of this pattern of splittings suggested refinement of the data in the *Immm* space group. However, Rietveld refinement of the powder X-ray data for the $x = 0.1$ sample in *Immm* produced an unsatisfactory fit. Detailed inspection of the single-phase Rietveld fit to the peaks which are split on lowering the symmetry to orthorhombic indicated that this was due to the presence of a small quantity of an undistorted tetragonal phase within the sample: the intensity does not fall to background level between them, suggesting that regions of the sample retain tetragonal symmetry (Figure 3b). Refinement was then attempted with a two-phase model, in which an undistorted *I*4/*mmm* structure is

(29) Crespin, M.; Bassat, J. M.; Odier, P.; Mouron, P.; Choisnet, J. *J. Solid State Chem.* **1990**, *84*, 165−170.
(30) Crespin, M.; Landron, C.; Odier, P.; Bassat, J. M.; Mouron, P.; Choisnet, J. *J. Solid State Chem.* **1992**, *100*, 281−291.

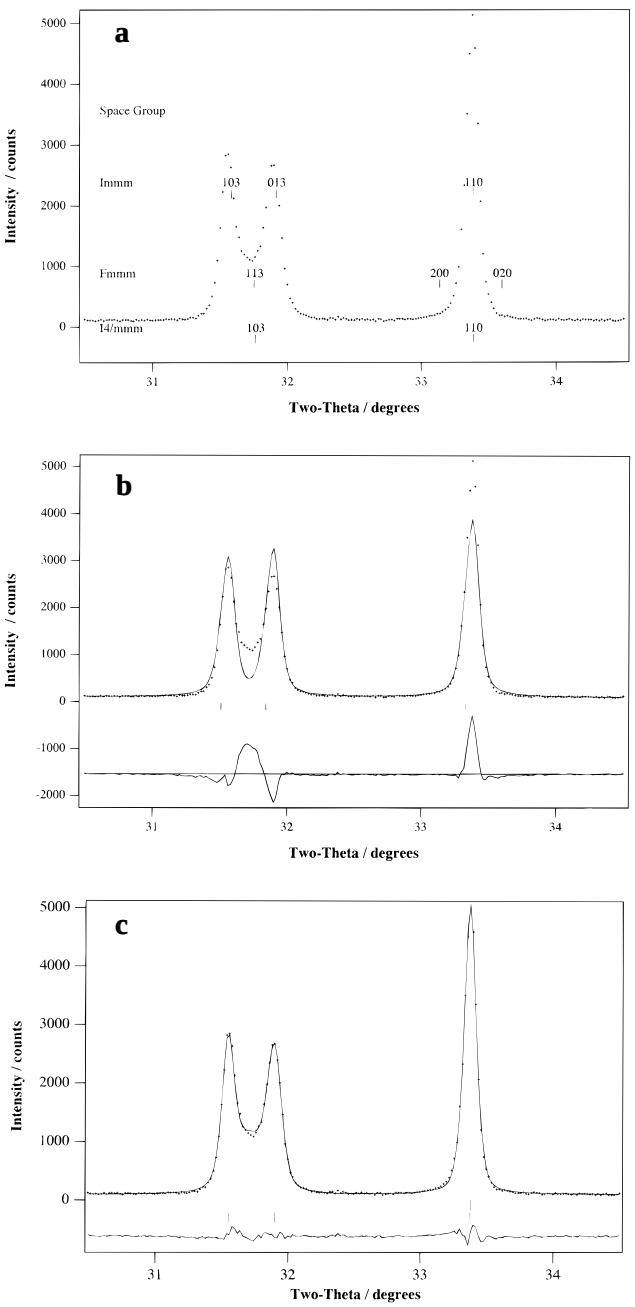

Figure 3. (a) Powder X-ray data for the tetragonal {103} and {110} reflections of $LaSrCr_{0.1}Ni_{0.9}O_{4+\delta}$ in *I*4/*mmm*, showing the positions of the peaks predicted in the alternative orthorhombic space groups *Immm* and *Fmmm*. (b) Section of the single-phase X-ray Rietveld refinement of $LaSrCr_{0.1}Ni_{0.9}O_{4+\delta}$ in *Immm*, presented as in Figure 2. (c) Section of the X-ray Rietveld refinement of $LaSrCr_{0.1}Ni_{0.9}O_{4+\delta}$ with one *Immm* and one *I*4/*mmm* phase, presented as in Figure 2.

introduced as a second phase. This resulted in a reduction of χ^2 from 2.9 to 2.1. The fit was still unsatisfactory, however, as the peak shape appeared to depend on the reflection Miller indices as well as the scattering angle. This was particularly true for the undistorted tetragonal phase.

Subsequent two-phase refinement of the data using the FullProf program enabled the use of microstrain broadening parameters for both phases, equivalent to allowing for a distribution of cell parameters within the sample,[27] and the inclusion of these terms resulted in a much improved fit, indicated by the further reduction in χ^2 to 1.3; the observed, calculated, and difference

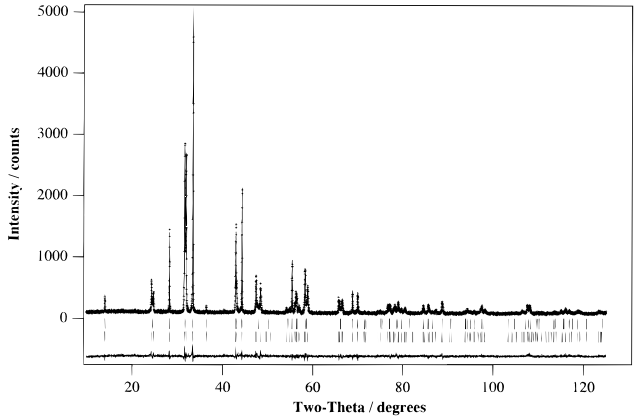

Figure 4. X-ray Rietveld refinement of $LaSrCr_{0.1}Ni_{0.9}O_{4+\delta}$ with one *Immm* and one *I*4/*mmm* phase, with anisotropic strain broadening used to calculate the *hkl* dependence of the reflection half-widths in both phases, presented as in Figure 2.

profiles for this refinement are shown in Figure 4. An enlargement of the fit to the 30.5−34.5° 2θ region is shown in Figure 3c and the corresponding structural parameters are given in Table 3. Three general anisotropic strain parameters, ϵ_i, for orthorhombic symmetry, one along each of the unit cell vectors ($\epsilon_i = \sigma_i/a_i$ where σ_i is the standard deviation of lattice parameter a_i), as previously used to describe the strain in $La_2NiO_{4\pm\delta}$, were employed to describe the Gaussian component of the strain for the *Immm* phase.[27] The values of 0.00044(1), 0.00067(3), and 0.000006(2) obtained for the *a*, *b*, and *c* parameters respectively indicate that the strain in this phase is basically confined to the MO_2 planes and slightly smaller in size than that reported for $La_2NiO_{4+\delta}$ (0.06).[27] The magnitude of the Gaussian component of the orthorhombic strain for the *a* parameter in the tetragonal phase was much greater, 0.019(2). Attempts to account for the observed peak shape anisotropy by using a Lorentzian component to model an anisotropic crystallite size distribution were unsuccessful. Refinement of the lattice parameters for the tetragonal *I*4/*mmm* phase and distorted, orthorhombic *Immm* phase led to the two phases having virtually identical *c* lattice parameters, while the *a* lattice parameter of the tetragonal phase is almost exactly half of the sum of the orthorhombic phase's *a* and *b* lattice parameters. The oxygen vacancies occur at the O(2) site which lies on the shorter of the axes in the MO_2 planes, and the equivalent site in the *I*4/*mmm* phase, whose composition was constrained to be the same as that of the majority orthorhombic phase (Figure 5).

The diffraction patterns of the other members of the series were then studied carefully to determine whether they showed any signs of such a distortion. The data for the $x = 0.2$ sample, which refined to $\chi^2 = 2.2$ in the tetragonal *I*4/*mmm* space group, was indeed found to be described more accurately by an approximately equimolar mixture of the undistorted, tetragonal *I*4/*mmm* phase and the distorted, orthorhombic *Immm* phase with virtually identical *c* lattice parameters. The *a* lattice parameter of the tetragonal phase is again almost exactly half of the sum of the orthorhombic phase's *a* and *b* lattice parameters, but the extent of the orthorhombic distortion is less than that found for the $x = 0.1$ sample. A multiphase refinement in which the profile coefficients of the two phases were con-

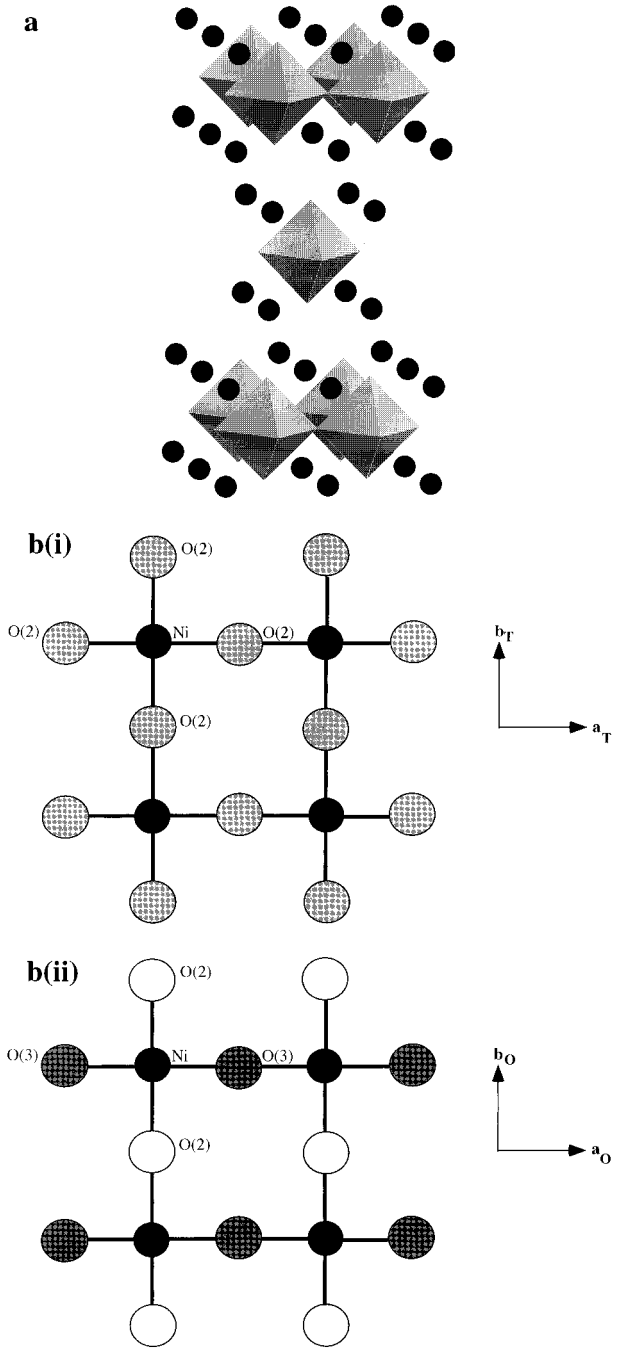

Figure 5. (a) K_2NiF_4 structure of $LaSrCr_xNi_{1-x}O_{4+\delta}$. (Ni/Cr)-$O_6$ octahedra are shown, and the La^{III}/Sr^{II} cations are represented as dark spheres. (b) Location of oxygen vacancies in the transition metal−oxygen layers of the tetragonal (*I*4/*mmm*) and orthorhombic (*Immm*) phases of the multiphase $x = 0.1$ and 0.2 samples; in the *I*4/*mmm* phase shown in (i), the oxygen vacancies are randomly distributed over the O(2) site and $a_T = b_T$, while in the *Immm* phase shown in (ii), the oxygen vacancies preferentially occur at the O(2) site leaving the O(3) site fully occupied. This results in a_O being greater than b_O ($a_T \approx [a_O + b_O]/2$).

strained to be the same and the oxygen temperature factors for the sites within the perovskite layers were constrained to be 0.02 Å^2 led to a highly significant reduction of χ^2 to 1.4, and a considerable improvement in the visual quality of the fit. Refinement of the oxygen fractional occupancies for the orthorhombic phase again indicated full occupancy of the (0,0,*z*) position but much reduced occupancy of the sites within the perovskite layers. Thus, the fractional occupancy of the former site was fixed at 1.0, while the occupancies of the latter sites were constrained to vary such that the overall oxygen stoichiometry in the orthorhombic phase was always in agreement with that obtained from the iodometry ($LaSrCr_{0.2}Ni_{0.8}O_{3.81}$; see Table 3). This led to a reduction in all the "goodness of fit" parameters and to, within error limits, full occupancy of the ($^1/_2$,0,0) oxygen position and reduced occupancy of the (0,$^1/_2$,0) position (see Figure 5b(ii)). Finally, in consideration of the virtually identical *c* lattice parameters and unit cell volumes of the two phases, the oxygen fractional site occupancy of the (0,$^1/_2$,0) position in the tetragonal *I*4/*mmm* phase was fixed at 0.905 so that the total oxygen content for this phase was the same as that for the orthorhombic phase. This led to a reduction in χ^2 to 1.3. Structural parameters obtained from the multiphase Rietveld refinement for the $x = 0.2$ sample are also given in Table 3. For both the $x = 0.1$ and 0.2 samples a preferred orientation correction in the [001] direction was refined for the *Immm* phase. [31,32]

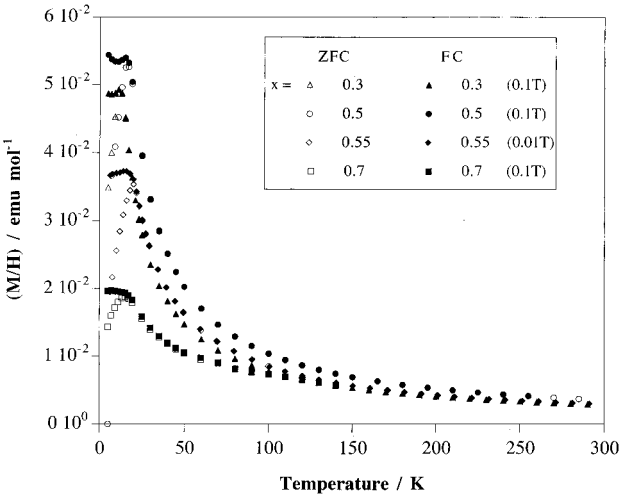

Figure 6. Molar magnetization versus temperature for $LaSrCr_xNi_{1-x}O_{4+\delta}$ samples with $x = 0.3$, 0.5, 0.55, and 0.7. The measuring fields are given.

Similar multiphase refinements indicated that the orthorhombic phase was not present in any of the samples with higher values of *x*, nor did the data for these samples refine satisfactorily in any other related lower symmetry space groups. However, this competition between the oxygen deficient tetragonal and orthorhombic phases may account for the unusual peak shapes, indicative of a multiphasic nature, encountered in the powder X-ray diffraction patterns of several compounds at intermediate stages of their preparation on the way to phase purity, as already discussed with respect to their synthesis.

Magnetic Measurements. Figure 6 shows the variation in the field cooled (FC) and zero-field cooled (ZFC) molar magnetization with temperature for $x = 0.3$, 0.5, 0.55, and 0.7.

The divergence of the FC and ZFC magnetization ($M_{FC} > M_{ZFC}$) for the $x = 0.3$, 0.5, 0.55, and 0.7 samples shows spin glass behavior with well-defined freezing temperatures, T_F, of between 12 and 19 K (see Table 4) while the $x = 0.9$ sample displays an antiferromagnetic

(31) Dollase, W. A. *J. Appl. Crystallogr.* **1986**, *19*, 267−272.
(32) March, A. *Z. Kristallogr.* **1932**, *81*, 285−297.

Table 4. Spin Glass Freezing Temperatures (T_F) Defined to within 2 K (One T Step) and Curie−Weiss Parameters for $LaSrCr_xNi_{1-x}O_{4+\delta}$ (x = 0.3, 0.5, 0.55, 0.7, and 0.9) and for $NdCaCr_{0.5}Ni_{0.5}O_4$ and $La_{0.9}Nd_{0.1}SrCr_{0.5}Ni_{0.5}O_4$

x (temperature range for Curie−Weiss fit)	T_F[a] (K)	C[b] (emu K/mol)	θ (K)	μ_{eff}/μ_B	μ_{theo}/μ_B
0.3 (30 → 300 K, 0.1 T)	12	0.86	−9.05	2.62	2.57
0.5 (25 → 300 K, 0.1 T)	16	1.06	−2.17	2.91	3.00
0.55 (20 → 300 K, 0.01 T)	19	0.87	−3.84	2.64	3.10
0.7 (30 → 140 K, 0.1 T)	15	1.09	−51.31	2.96	3.38
0.9 (165 → 300 K, 0.1 T)		1.13	−253.41	3.00	3.71
$NdCaCr_{0.5}Ni_{0.5}O_4$ (20 → 300 K, 0.01 T)	19	2.16	−3.32	4.16	4.69
$La_{0.9}Nd_{0.1}SrCr_{0.5}Ni_{0.5}O_4$ (20 → 300 K, 0.1 T)	16	1.18	−4.89	3.08	3.21

[a] T_F determined from change of sign in plots of $\partial\chi/\partial T$ versus T and the divergence between the ZFC and FC magnetization. [b] Curie−Weiss fits to the equation $\chi = C/(T - \theta)$ where $C = N_a\mu_B^2\mu_{eff}^2/3k_B$.

transition with a Neel temperature, T_N, of 150 K (determined from the maximum in a plot of $\partial\chi/\partial$T versus T) and is a weak ferromagnet below ∼130 K. Above T_F and T_N, respectively, the susceptibilities follow the Curie−Weiss law and the calculated values of the Curie constant (C), Weiss constant (θ), and magnetic moment (μ_{eff}) are given in Table 4. Measurement of linear M(H) isotherms at 298 K indicated that all the compounds were conventional paramagnets above their ordering/freezing temperatures.

Reduction. In an attempt to determine the oxygen stoichiometry of the samples and to reveal the presence of any stable oxygen deficient species the compounds were reduced under flowing dry H_2 at 800 °C. Complete reduction to nickel and chromium metal did not occur for any value of x, but partial reduction was observed, the percentage weight loss depending crucially upon the chromium-to-nickel ratio; the larger x, the smaller the percentage lost. Results are summarized in Table 5. Further experiments in which samples were heated at temperatures of up to 1000 °C for periods of up to 12 h still did not result in the complete reduction to chromium and nickel metal of any of the compounds studied. This behavior is in contrast to that of both the parent all-nickel and all-chromium compounds; the former are reduced completely according to the following reaction scheme, at temperatures of less than 800 °C,[5,9] while the latter are not reduced at all under the conditions employed:[17]

$$La_{2-x}Sr_xNiO_{4\pm\delta} \rightarrow {}^1/_2(2 - x)La_2O_3 + xSrO + Ni + (1 + x/2 \pm \delta)H_2O$$

The experiments described above were also repeated using 8% H_2 in Ar rather than pure hydrogen, and in all cases this simply resulted in an increase in the temperature at which reduction began to occur and a decrease in the extent of reduction observed by roughly 20% for any given temperature.

For samples with $x \neq 0.5$ the thermogravimetric analysis (TGA) traces consist of several gradual reduction steps, but no clear plateaux indicative of possible metastable intermediates (see Figure 7a,b for the traces for the x = 0.3 and x = 0.7 samples, respectively). Although the extent of reduction increases with temperature and time, the kinetics are sufficiently slow that complete reduction is never achieved under the conditions used. The products are black, and powder X-ray diffraction indicates that the K_2NiF_4 structure is retained. In fact reduction always results in a mixture of Ni^{II} and Ni^{I} (Table 5), i.e., reduction past the Ni^{I} oxidation state is not observed.

Table 5. Summary of Thermogravimetric Analysis Data for the Reduction of $LaSrCr_xNi_{1-x}O_{4+\delta}$ Samples (x = 0.3, 0.5, 0.7, and 0.8) under Dry, Flowing H_2 at 800 °C[a]

x	δ	% mass lost at 800 °C	oxygens per formula unit lost	composition of reduction product	Ni oxidation state in reduction product
0.3	−0.08	2.51	0.54	$LaSrCr_{0.3}Ni_{0.7}O_{3.38}$	+1.23
0.5	0.03	2.51	0.54	$LaSrCr_{0.5}Ni_{0.5}O_{3.49}$	+0.96
0.7	0.04	1.53	0.33	$LaSrCr_{0.7}Ni_{0.3}O_{3.71}$	+1.07
0.8	0.04	1.08	0.23	$LaSrCr_{0.8}Ni_{0.2}O_{3.81}$	+1.10

[a] The Ni oxidation state in the reduction products is calculated on the assumption that the chromium is not reduced below Cr^{III}.

However, for the x = 0.5 sample reduction occurred in a single sharp step at ∼450 °C, with a decrease in mass corresponding to loss of half an oxygen per formula unit, i.e., to formation of the kinetically stable product $La_2Sr_2CrNiO_7$, which was brown (see Figure 7c). By exposure of this reduced phase to the laboratory atmosphere while still in the thermogravimetric apparatus, it was established that the product was air stable at ambient temperatures.

To enable the reduction product to be studied further, a bulk sample was produced. $LaSrCr_{0.5}Ni_{0.5}O_4$ (2 g) was placed in an alumina boat and placed in a tube furnace which was then purged with hydrogen for approximately 30 min. The sample was then heated at 5 °C min^{-1} to 600 °C under the hydrogen flow and left at this temperature for 4 h before being allowed to cool to room temperature over a period of 3 h. Powder X-ray diffraction data were collected, as previously described, and the pattern obtained showed no signs of any impurity phases. Attempts were made to refine the data in several space groups: refinement in $I4/mmm$ produced a poorer fit than that obtained in $Fmmm$ while refinements in $P4_2/ncm$, $Immm$, $Cmca$, and $Pccn$ proved unstable. The structural parameters obtained from Rietveld refinement of the data using the $Fmmm$ orthorhombic space group are given in Table 6 and the observed, calculated and difference profiles in Figure 8.

Refinement of the oxygen site occupancies led to full occupancy of the (0,0,z) position, and so the fractional occupancy of this site was fixed at 1.0, but to greatly reduced occupancy of the oxygen site within the transition-metal layers at ($^1/_4$,$^1/_4$,0), leading to a calculated oxygen deficiency, δ, of 0.32. Clearly this is less than the value of 0.5 obtained from thermogravimetric analysis but is consistent with reduction in the transition-metal oxidation state by loss of oxygen solely from within the perovskite layers. The observation that fixing the fraction to 0.75 in accordance with the TGA data leads to a change of less than 1.5% in χ^2 indicates

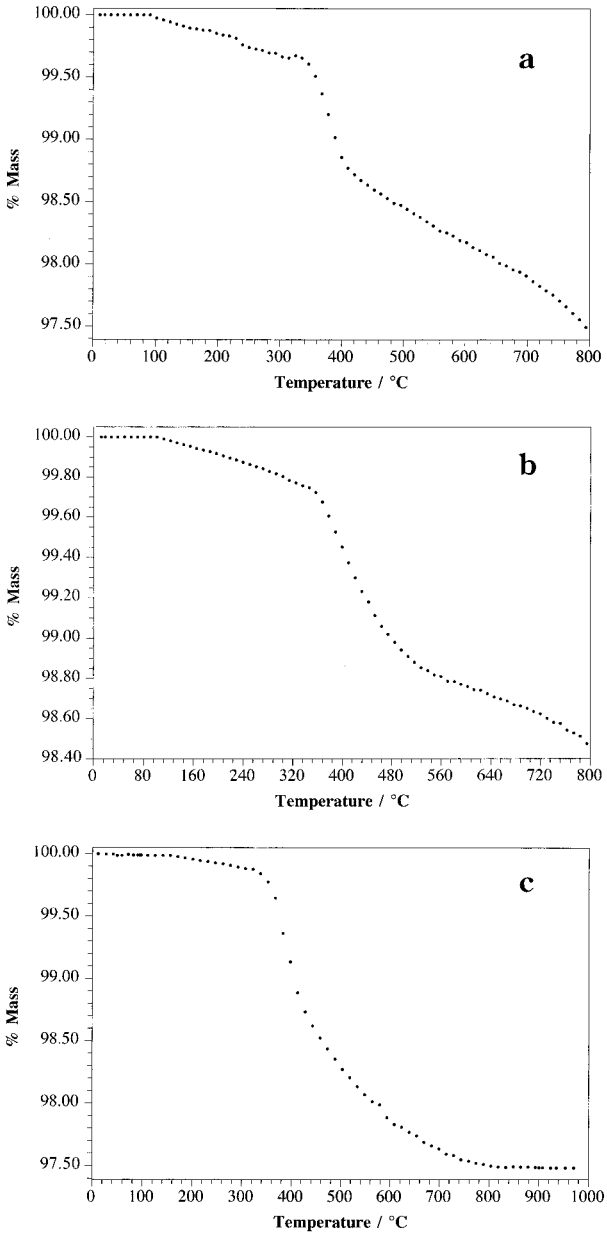

Figure 7. (a) Thermogravimetric analysis (TGA) of $LaSrCr_{0.3}Ni_{0.7}O_{3.92}$ under a flowing hydrogen atmosphere. (b) TGA of $LaSrCr_{0.7}Ni_{0.3}O_{4.04}$ under a flowing hydrogen atmosphere. (c) TGA of $LaSrCr_{0.5}Ni_{0.5}O_{4.03}$ under a flowing hydrogen atmosphere.

the relative lack of sensitivity of powder X-ray diffraction to the precise oxygen content.

Discussion

The criterion for the successful synthesis of a single phase has to be rigorously applied in this phase field through detailed inspection of Rietveld refinements of the products—powder X-ray diffraction patterns of many samples, which on visual inspection appear phase pure, reveal unusual peak shapes that cannot be fitted to a single-phase structural model on refinement, indicating that secondary phase(s) with very similar structures and lattice parameters must also be present. Subsequent annealing of these samples at 1200−1300 °C in argon generally removed this feature from the X-ray diffraction patterns and single-phase Rietveld refinement of the data obtained gave satisfactory fits, indicating

Table 6. Structural Parameters Obtained from the Rietveld Refinement of Powder X-ray Diffraction Data for $La_2Sr_2CrNiO_7$[a]

		$La_2Sr_2CrNiO_7$
a (Å)		5.4336(1)
b (Å)		5.4280(1)
c (Å)		12.6104(2)
V (Å^3)		371.93
La/Sr	z	0.35932(9)
	U_{iso} (Å^2)	0.0081(5)
Cr/Ni	U_{iso} (Å^2)	0.012(1)
O(1)	z	0.1677(6)
	U_{iso} (Å^2)	0.010(2)
O(2)	U_{iso} (Å^2)	0.010(2)
	occupancy	0.84(1)
R_{wp} (%)		9.5
R_p (%)		7.4
R_F^2 (%)		9.2
R_F (%)		3.7
χ^2		1.2
bond length (Å)	Ni/Cr−O(1) × 2	2.115(8)
	Ni/Cr−O(2) × 4	1.92010(4)

[a] The atoms were refined in the following Wyckoff positions of space group No. 69, *Fmmm*:

8(La/Sr) and 8O(1)	in (i)	(*mm*2)	(0,0,*z*)
4(Ni/Cr)	in (a)	(*mmm*)	(0,0,0)
8O(2)	in (e)	(2/*m*)	($^1/_4$,$^1/_4$,0)

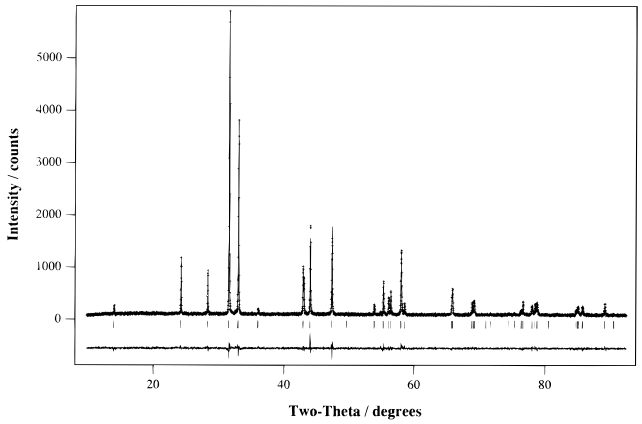

Figure 8. X-ray Rietveld refinement of $La_2Sr_2CrNiO_7$ in *Fmmm*, presented as in Figure 2.

insufficient high-temperature annealing under argon initially. The difficulty in forming a single phase may be qualitatively attributable to the conflicting requirements of the different oxidation states which need to be stabilized. The iodometric measurement of the oxygen content (which was not possible by thermogravimetric analysis as complete reduction does not occur) indicates the evolution of oxidation state with chromium content, x.

As the percentage chromium content, x, is decreased, i.e., as the percentage nickel content is increased, the total oxygen content of the samples, and thus the average transition-metal oxidation state, decreases quite dramatically (see Figure 1); samples containing 50% nickel and 50% chromium are approximately stoichiometric: the small amounts of excess oxygen for $x \geq 0.5$ may be attributed to partial oxidation from Cr^{III} to Cr^{IV} ($\delta = 0.03/0.04$), whereas the sample with 90% nickel and 10% chromium contains only 3.75 oxygens per formula unit ($\delta = -0.25$). It is clear that the greater the proportion of nickel in the samples, the more difficult is the total formation of Ni^{III} from Ni^{II} under the synthesis conditions. The small deviations in the oxygen stoichiometry from 4.00 for the samples with x

≥ 0.3 indicates exclusive formation of Ni^{III}, which is at first sight surprising given that the phases can be prepared only under argon. Increasing the concentration of chromium cosubstituted on the octahedral site clearly enhances the stability of Ni^{III}. This may be explained in terms of the less electronegative nature of Cr^{III} compared with Ni^{III}. Competition for donation from the oxide anion to a Ni^{III} center is reduced as the Cr^{III} concentration increases; the $Cr^{III}-O$ bond is more ionic, and thus Ni^{III} is stabilized via increased covalency with the oxide anion. At lower Cr^{III} concentrations ($x \leq 0.2$), the Ni^{III} oxidation state is not stable under these reaction conditions and oxygen vacancies form under the argon synthesis atmosphere. The tendency of these vacancies to order crystallographically results in the ordered *Immm* structure forming in competition with the disordered *I*4/*mmm* structure in a two-phase sample. Here and in the rest of the paper we use the term "ordered" to indicate the preferential location of the oxygen vacancies along the *b* axis of the *Immm* structure—there is no evidence for ordering of the vacancies along this direction.

Inspection of the lattice parameters for the orthorhombic and tetragonal phases in the multiphase $x = 0.1$ and 0.2 samples suggests an interesting defect chemistry: the *c* lattice parameters and unit cell volumes of the vacancy-ordered orthorhombic and disordered tetragonal phases are essentially identical within the error limits of the refinement, while the *a* lattice parameter of the tetragonal *I*4/*mmm* phase is found to be equal to half the sum of the *a* and *b* lattice parameters of the orthorhombic *Immm* phase. The close structural relationship between the two phases would imply that they arise from regions of the sample with the same chemical composition, including oxygen concentration, but in which the oxygen vacancies are ordered (orthorhombic phase) or disordered (tetragonal phase): refinement of powder X-ray diffraction data is relatively insensitive to the oxygen content of the minority tetragonal phase. Refinement of the oxygen site fractions for the major orthorhombic phase, 61.5% and 58.1% for $x = 0.1$ and 0.2, respectively, results in full occupancy of the (0,0,*z*) and ($^1/_2$,0,0) positions, but much reduced occupancy of the (0,$^1/_2$,0) site within the transition-metal layers. It would appear therefore that it is the presence and ordering of these oxygen vacancies that is the driving force for the structural distortion (as for $La_{1.6}Sr_{0.4}(Ni^{I},Ni^{II})O_{3.47}$[29] and $LaSr(Ni^{I},Ni^{II})O_{3.1}$[30]) and the quantity of tetragonal material remaining in the sample is highly strained, producing the anisotropic peak broadening observed in the diffraction pattern for the $x = 0.1$ sample. The facts that the extent of the orthorhombic distortion is less for the $x = 0.2$ phase than for $x = 0.1$ and that refinement of the powder X-ray diffraction data for the former sample did not require the use of anisotropic microstrain parameters are consistent with the presence of fewer oxygen vacancies as the nickel concentration is decreased. Efforts to isolate either phase in pure form have proved unsuccessful.

A decrease in *c* but an increase in *a* and the unit cell volume are observed with increasing chromium content, *x*; plots of *a*, *c*, *c*/*a*, and unit cell volume vs *x* are shown in Figure 9a–c, respectively. Figure 10a,b shows plots of the axial and equatorial Ni/Cr–O bond lengths versus *x* and the ratio of the difference and sum of these two

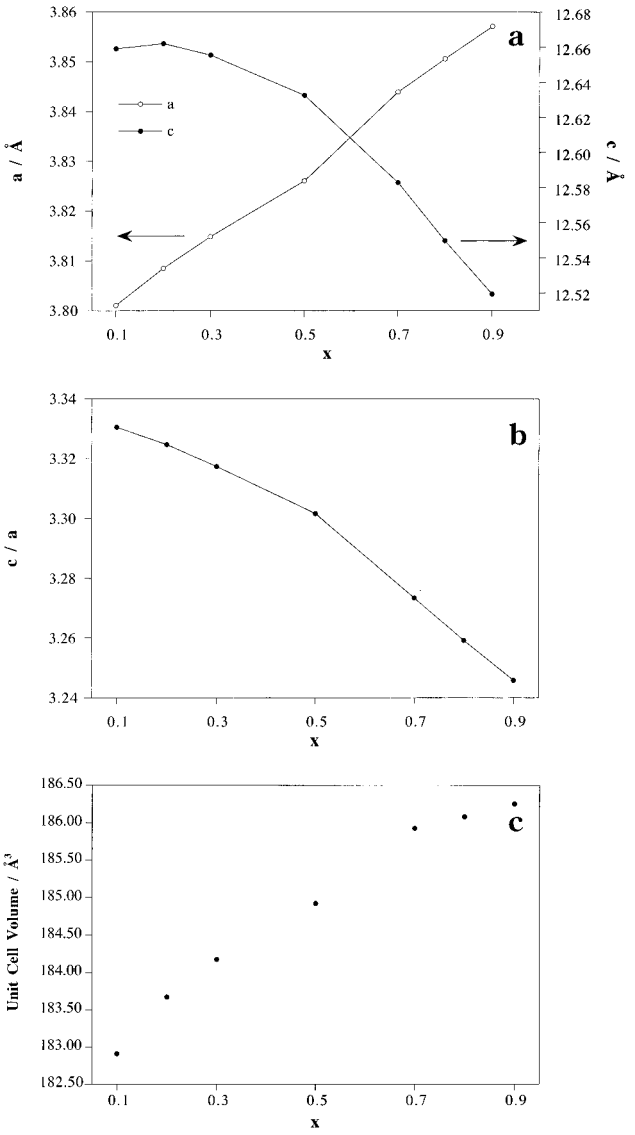

Figure 9. (a) Plot of *a* and *c* lattice parameters versus *x* for $LaSrCr_xNi_{1-x}O_{4+\delta}$ (average tetragonal values used for the $x = 0.1$ and 0.2 samples, here, and in Figures 9b,c and 10a,b). (b) Plot of *c*/*a* versus *x* for $LaSrCr_xNi_{1-x}O_{4+\delta}$. (c) Plot of unit cell volume versus *x* for $LaSrCr_xNi_{1-x}O_{4+\delta}$.

bond lengths versus *x*, respectively. The steady decrease in *c*/*a* and the variation in the axial (decreases) and equatorial (increases) transition metal–oxygen bond lengths with increasing chromium content, *x*, are consistent with a decrease in the extent of the Jahn–Teller distortion of the MO_6 octahedra with decreasing Ni^{III} concentration. However for low *x*, the samples are highly oxygen deficient and a significant percentage of the nickel in these compounds is present as Ni^{II}; thus as *x* increases not only does the amount of chromium in the samples increase, and hence the amount of nickel decrease, but also the oxidation state of the nickel increases such that for $x \geq 0.5$ all the nickel is present as Ni^{III}. The observed distortion of the octahedra is consistent with ordering of the hole in the e_g^1 configuration in the d_{z^2} orbital. The unit cell volume also increases with *x* in the $LaSrCr_xNi_{1-x}O_4$ series, rather than decreasing, but the rate of increase seems to decline as *x* becomes larger. Qualitatively such an increase may be expected, assuming an ionic model,

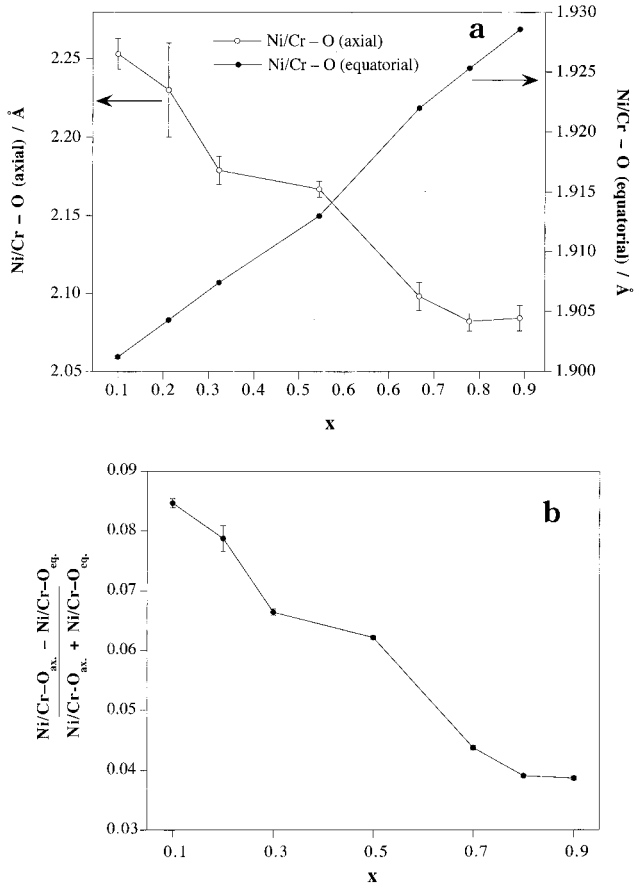

Figure 10. (a) Plot of axial and equatorial Ni/Cr−O bond lengths versus x for $LaSrCr_xNi_{1-x}O_{4+\delta}$. (b) Plot of the ratio of the sum and difference of the axial and equatorial Ni/Cr−O bond lengths versus x for $LaSrCr_xNi_{1-x}O_{4+\delta}$.

according to the larger effective ionic radius of six-coordinate Cr^{III} (0.615 Å) compared to that of Ni^{III}, whether high (0.60 Å $t_{2g}^5e_g^2$) or low (0.56 Å $t_{2g}^6e_g^1$) spin in an oxide environment.[33,34] The apparent breakdown of Vegard's law for low nickel concentrations (high x) as previously observed in the three-dimensional perovskite solid solution $LaCr_xNi_{1-x}O_3$[18,20] could simply be explained by the short-range ordering of transition-metal cations within the samples or in terms of the different oxygen concentrations.

The magnetic properties of the system change significantly as the chromium concentration increases. Comparison of the observed magnetic moments with calculated values shows that the susceptibility is consistent with localized Ni^{III} and Cr^{III} for all the compounds in the series and that the d^7 Ni^{III} cation is present in a low-spin state, commonly found in oxides. This is consistent with the interpretation of the evolution of the shape of the MO_6 octahedron in terms of a Jahn−Teller distortion due to low-spin Ni^{III}.

$La_2NiO_{4\pm\delta}$ orders antiferromagnetically above room temperature when stoichiometric and at lower temperatures when $\delta > 0$, in much the same way as $La_2CuO_{4\pm\delta}$. In both systems the strong interactions of the hole introduced upon substitution with the neighboring Cu^{II} or Ni^{II} spins results in the rapid destruction of long-range antiferromagnetic order. The magnetic susceptibility near $x = 1$ in $La_{2-x}Sr_xNiO_4$ is small in overall magnitude and only weakly temperature dependent, with no sign of magnetic ordering.[9] The compounds studied here result from substitution of Cr^{III} into the Ni^{III} phase $LaSrNiO_4$. $LaSrNiO_4$ itself is very difficult to prepare as a truly single phase[35] and is highly conducting with a small magnetic susceptibility ($\chi = (4-5) \times 10^{-4}$ emu mol^{-1} [6,9]) which is temperature independent below room temperature and shows a broad maximum at 650 K which has been attributed to the 2D antiferromagnetic interaction between low-spin Ni^{III} cations—the increase in both the magnitude and temperature dependence of χ on Cr^{III} substitution can then be understood as being due to either localization of the delocalized Ni^{III} electrons or disruption of the antiferromagnetic exchange interactions in the parent by the introduction of the competing interactions discussed below upon substitution.

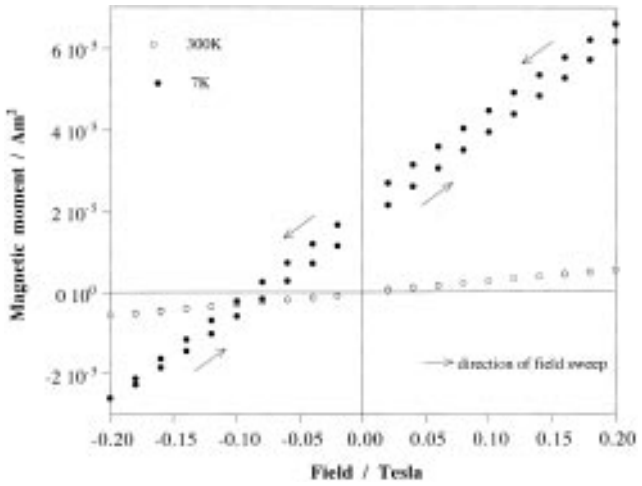

Figure 11. Field-cooled magnetization hysteresis loops at room temperature and 7 K for $LaSrCr_{0.55}Ni_{0.45}O_{4.04}$.

In addition to the effect of substitution on the paramagnetic phase, the square array of localized Cr^{III} and Ni^{III} cations displays the cooperative magnetic properties characteristic of a spin glass (a random, yet cooperative freezing of spins at a well-defined temperature, T_F, producing a highly irreversible, metastable state without the long-range spatial order found in ferro- or antiferromagnetic systems[36]) at low temperature, i.e., divergence of the field-cooled and zero-field dc susceptibilities below the freezing temperature T_F. The spin glass behavior suggested by the ZFC/FC magnetization hysteresis was confirmed for the $x = 0.55$ sample by carrying out field-cooled hysteresis measurements at room temperature and 5 K (Figure 11). The room-temperature loop shows no hysteresis and passes through the origin as expected for a simple paramagnet, while the 5 K data show hysteresis with the resulting loop being displaced from the origin. This displacement is a clear indication of spin glass behavior and rules out the possibility of weak ferromagnetism: in this case the hysteresis loop would be symmetric about the origin. The observed hysteresis in both spin glasses and weak ferromagnets is due to uniaxial anisotropy, but the unidirectional anisotropy unique to the spin glass state

(33) Shannon, R. T.; Prewitt, C. T. *Acta Crystallogr.* **1969**, *B25*, 925−946.
(34) Shannon, R. T.; Prewitt, C. T. *Acta Crystallogr.* **1970**, *B26*, 1046−1048.
(35) Millburn, J. E.; Rosseinsky, M. J. unpublished results.
(36) Mydosh, J. A. *Spin glasses: an experimental introduction*; Taylor & Francis: London, 1993.

produces the characteristic displacement of the loop from the origin. Further confirmation of spin-glass behavior comes from consideration of the field dependence of the freezing temperature. Comparison of susceptibility data collected in different magnetic fields for the $x = 0.55$ and $NdCaCr_{0.5}Ni_{0.5}O_4$ shows that as the magnitude of the field increases, the value of the freezing temperature decreases. This is to be expected qualitatively as the larger the field the greater the inclination of the blocks to orientate themselves with it and hence the lower the temperature required before the interactions between the clusters results in freezing: quantitatively we expect $T_F \propto B^{-2/3}$.

Spin-glass behavior is generally agreed to require both disorder and frustration—the disorder clearly arises from the presence of both Cr^{III} and Ni^{III} on the octahedral site, but the square lattice is not intrinsically geometrically frustrated and careful consideration of the products of possible Cr^{III}/low-spin Ni^{III} 180° superexchange around a square plaquette is required to understand the observed spin glass behavior. The following discussion assumes that the M−O−M bond angles within the MO_2 array are 180°: this appears to be the *average* angle from X-ray diffraction, although this technique would certainly not be sensitive to small, uncorrelated local displacements which would influence the magnetism. Mossbauer measurements show that the sign of the Fe^{3+}−O−Cr^{3+} superexchange interaction depends critically on the size of the bond angle, being antiferromagnetic when the angle is less than 162° and ferromagnetic for angles closer to 180°.[37] Cr^{III}−O−Cr^{III} interactions are clearly antiferromagnetic, both from the Goodenough−Kanamori predictions for d^3−d^3 coupling and the observed antiferromagnetism of $LaSrCrO_4$. Ni^{III}−O−Cr^{III} (d^3−d^7) coupling is ferromagnetic due to the e_g contribution which operates in second order by Hund's rule coupling of the e_g electrons to the t_{2g} electrons in the excited state. Ni^{III}−O−Ni^{III} (d^7−d^7) interactions could in principle have either sign, depending on the presence and relative orientation of Jahn−Teller orbital ordering at the two coupled cations. Octahedral d^7−d^7 coupling or that involving overlap between the half-filled and empty orbitals of two Jahn−Teller distorted cations will be ferromagnetic, while that between the two half-filled nondegenerate orbitals of Jahn−Teller distorted cations will be antiferromagnetic. A square plaquette of 2 Cr^{III} and 2 Ni^{III} cations in which each Cr^{III} has one Ni^{III} and one Cr^{III} neighbor is frustrated if the Ni−Ni interaction is ferromagnetic (a plaquette is defined to be frustrated if the product ΠJ_{ij} of the exchange interactions around the loop is −1). The introduction of competing ferromagnetic interactions into the square antiferromagnetic array is thus capable of producing the frustration required for spin glass behavior, which is also found in the K_2NiF_4 structure mixed-metal fluoride $Rb_2Cu_{1-x}Co_xF_4$[38,39]—in this case the relative local orientation of empty orbitals on the Jahn−Teller active Cu^{II} cation is important in achieving frustration, and no long-range Jahn−Teller orbital ordering is required for spin glass behavior.

The $x = 0.9$ sample displays an antiferromagnetic transition at 150 K rather than a spin glass-like freezing point. Below 130 K the susceptibility rises, indicating a weak ferromagnetic component due to spin canting of the antiferromagnetically ordered chromium ions at ~130 K, as has been previously reported for the orthorhombic $LnCaCrO_4$ compounds, which order antiferromagnetically above room temperature.[17,40] 10% Ni^{III} substitution is therefore insufficient to fully frustrate long-range antiferromagnetic ordering and merely serves to reduce the Neel temperature from above 300 to 150 K. The larger value of the Weiss constant, θ, for this phase (see Table 4) than for the spin glasses found for lower values of x is quite consistent with the observation of antiferromagnetic long-range order and reduced frustration here.

Consideration of the data for the neodymium-containing compounds indicates that the above conclusions concerning the magnetism in the MO_2 planes are independent of the nature of the rare-earth cation. The large moment (3.6 μ_B) of Nd^{III} swamps that of the transition metals and the freezing of moments in the perovskite layers appears only as a point of inflection in the susceptibility versus temperature curves. Above T_F the susceptibility can be fitted to the Curie−Weiss law, and the values obtained are given in Table 5. The fact that the values of T_F for these compounds are of the same order as those for the samples containing a nonmagnetic lanthanide cation (La^{III}) indicates that the electronic nature of the ion in the rock salt layers has little, if any, influence upon the freezing process, i.e., there is weak coupling between the rock salt Ln^{III} moments and those of the transition-metal cations.

In the $La_{2-x}Sr_xNiO_4$ series, irreversible magnetism characteristic of a spin glass is observed for $x \leq 1.0$, i.e., before the metal−insulator transition. The results on the present system show that disorder and competing interactions can produce canonical spin glass behavior in a two-dimensional square array of truly localized electrons. As the introduction of Ni^{III} into La_2NiO_4 will, in the localized electron limit, also produce competing exchange interactions, the origin of the magnetism in the pure nickelates before the onset of metallic behavior may be similar to that found here.

The reduction chemistry of these mixed Cr^{III}/Ni^{III} phases is quite different from that of the pure end-members, with reduction beyond the Ni^{I} oxidation state being very strongly inhibited. The reduction in oxygen content indicated by the weight loss must be accompanied by a decrease of the combined transition-metal charge by one unit in order to preserve overall charge neutrality. There are a number of ways in which this could occur:

(1) The reduction could occur entirely at the chromium resulting in a Cr^{I}/Ni^{III} compound—this possibility can be discounted since there are no reported occurrences of chromium in the +1 oxidation state in an oxide environment.

(2) The reduction in charge could be split evenly between the chromium and nickel resulting in a Cr^{II}/Ni^{II} compound—this seems unlikely. First, there are no examples of well-characterized oxides containing Cr^{II},

(37) Gibb, T. C. *J. Chem. Soc., Dalton Trans.* **1984**, *4*, 667−671.
(38) Dekker, C.; Arts, A. F. M.; de Wijn, H. W. *Phys. Rev. B* **1988**, *38*, 8985−8991.
(39) Dekker, C.; Arts, A. F. M.; de Wijn, H. W. *Phys. Rev. B* **1988**, *38*, 11512−11522.
(40) Romero, J.; Saez Puche, R.; Fernandez, F.; Martinez, J. L.; Chen, Q.; Castro, M.; Burriel, R. *J. Alloys Compounds* **1995**, *225*, 203−207.

and second because the parent all-chromium oxide, $LaSrCrO_4$, cannot be reduced below Cr^{III} at all in this manner. In contrast the all-nickel compounds can be reduced below Ni^{II}.

(3) Reduction could occur entirely at nickel resulting in a Cr^{III}/Ni^{I} compound—this is the most probable explanation, as there are several known Ni^{I} oxides that have been produced by the hydrogen reduction of more oxidized species.[14,15,41] This view is consistent with the percentage weight loss decreasing with increasing x, i.e., decreasing as the percentage of nickel in the sample is decreased and with the stability of Cr^{III} in $LaSrCrO_4$ under H_2 at up to 1000 °C. The unusual property of the material produced here is its exceptional thermal stability. All the Ni^{I} oxides previously reported in the literature have been identified merely as brief, metastable plateaux in the overall reduction process, making bulk isolation of the specific monovalent product difficult. There are no such problems in our synthesis as reduction does not proceed past the Ni^{I} state. The reason for this would appear to be the stabilizing influence of the Cr^{III} ions; any further reduction must either occur at the chromium or result in the expulsion of Ni metal, which would destroy the K_2NiF_4 structure. This is clearly very unfavorable for Cr^{III} as indicated by the lack of reactivity with respect to reduction of the $LnSrCrO_4$ oxides. Thus the presence of the electropositive Cr^{III} cation is effective in stabilizing the otherwise transient Ni^{I} oxidation state, presumably by reducing the rate of reduction of the K_2NiF_4 structure.

The structural data obtained for the hydrogen reduction product of the $x = 0.5$ sample is consistent with the formation of $La_2Sr_2Cr^{III}Ni^{I}O_7$; refinement of the oxygen site occupancies leads to a reduced oxygen concentration compared to the starting material and these oxygen vacancies occur solely in the transition metal−oxygen layers. If the equatorial $Cr^{III}/Ni^{I}-O(2)$ bond length of 1.92010(4) Å (see Table 6) is compared with that for the unreduced $x = 0.5$ sample of 1.91303(2) Å, there is a clear increase upon reduction as expected since the ionic radius of Ni^{I} will be greater than that of Ni^{III}.

The general approach of introducing an electropositive species into the structure to kinetically stabilize the Ni^{I} oxidation state thus appears promising. To explore the correspondence between the d^9 ions, Ni^{I} and Cu^{II}, the aim is to prepare stable, contiguous arrays of Ni^{I}: to obtain metallic behavior the disordered arrangement of the transition-metal cations over the octahedral sites found in the current system must be avoided. The use of a precursor structure with an ordered array of Ni^{III} and the more electropositive cations in different sites within the unit cell (ideally an ordered layered structure) would both afford the desired kinetic stability against reduction beyond Ni^{I} and allow the observation of the properties of this oxidation state in a thermally stable system free from disorder.

Acknowledgment. The authors would like to thank the donors of the Petroleum Research Fund, administered by the American Chemical Society, and UK EPSRC for financial support. We are grateful to Dr. J. P. Attfield and Prof. P. Day for allowing us access to the SQUID magnetometers at the IRC in Superconductivity at the University of Cambridge and the Royal Institution, respectively. We would also like to thank Dr. M. A. Green (ICL, Oxford) for introducing us to the Fullprof program and for many other useful discussions.

CM960357V

(41) James, M.; Attfield, J. P. *Physica C* **1994**, *235*, 751−752.